Journal of Power Sources 377 (2018) 1–6

Contents lists available at ScienceDirect

Journal of Power Sources

journal homepage: www.elsevier.com/locate/jpowsour

Improving cycle stability of SnS anode for sodium-ion batteries by limiting Sn agglomeration

Wenhui Wang[a], Liang Shi[a,b], Danni Lan[a], Quan Li[a,*]

[a] Department of Physics, The Chinese University of Hong Kong, Shatin, New Territory, Hong Kong, China
[b] Department of Chemistry, University of Science and Technology of China, Hefei, 230026, China

HIGHLIGHTS

- Flower-like SnS nanostructures are obtained by a simple solvothermal method.
- Sn agglomerates in SnS anode for Na-ion batteries upon cycling.
- Sn agglomeration correlates well with the capacity decay of SnS.
- MWCNT effectively suppress Sn agglomeration and improve cyclability of SnS.
- $Na_{2/3}Ni_{1/3}Mn_{1/2}Ti_{1/6}O_2$/SnS-MWCNT full cell delivers an energy density of 262 Wh/kg.

ARTICLE INFO

Keywords:
Sodium ion battery
Anode
SnS
Tin agglomeration
Cycle stability
Carbon nanotubes

ABSTRACT

Flower-like SnS nanostructures are obtained by a simple solvothermal method for anode applications in Na-ion batteries. We show experimental evidence of progressive Sn agglomeration and crystalline Na_2S enrichment at the end of de-sodiation process of the SnS electrode, both of which contribute to the capacity decay of the electrode upon repeated cycles. By replacing the commonly adopted acetylene black conductive additive with multi-wall carbon nanotubes (MWCNT), the cycle stability of the SnS electrode is largely improved, which correlates well with the observed suppression of both Sn agglomeration and Na_2S enrichment at the end of de-sodiation cycle. A full cell is assembled with the SnS/MWCNT anode and the P2-$Na_{2/3}Ni_{1/3}Mn_{1/2}Ti_{1/6}O_2$ cathode. An initial energy density of 262 Wh/kg (normalized to the total mass of cathode and anode) is demonstrated for the full cell, which retains 71% of the first discharge capacity after 40 cycles.

1. Introduction

Room temperature sodium-ion battery (SIB) has been considered as a promising alternative for lithium-ion battery (LIB) in large-scale electric energy storage applications, due to the natural abundance and uniform distribution of Na on earth [1,2]. However, its practical application remains challenging due to the limited choices of anode materials with high energy density and good cycle stability.

The high theoretical capacity of SnS (~1022 mAh/g) makes it a promising candidate for anode applications in SIBs [3–5]. Cao's group firstly tested SnS-based anode in SIB [6]. The reported Sn-SnS-20 wt%C nanocomposite can deliver an initial de-sodiation capacity of 333 mAh/(g composite) with capacity retention of 87% over 150 cycles at 70 mA/g. SnS@graphene (13.8 wt%) composite has first de-sodiation capacity of 1037 mAh/g at 30 mA/g and retained ~90% of the capacity after 50 cycles [4]. Okada's group investigated the effect of hard carbon (HC) and graphene (G) on the electrochemical performance of SnS [7]. The optimized composite, SnS/(13.5 wt%G+10 wt%HC), shows a reversible capacity of 598 mAh/g with a capacity retention of ~87% after 30 cycles at 50 mA/g. Most recently, Kang' group demonstrated that a 3D SnS flower free of carbon can deliver a capacity of 432 mAh/g, with a retention of ~72% after 50 cycles at 150 mA/g [8]. To date, the cycle performance of the SnS based anode remains unsatisfactory. More importantly, the detailed mechanism of capacity decay of SnS was not understood, but intuitively ascribed to the large volume changes (the final volume, by assuming the Na_2S and $Na_{15}Sn_4$ as the final sodiated products, versus pristine volume is estimated as 442%) upon cycling.

In this work, we investigated the microstructure and phase evolution of the SnS anode upon cycling, when capacity fading occurs. Progressive Sn agglomeration and enrichment of Na_2S at the end of de-sodiation process are observed, which provided an explanation to the

* Corresponding author.
E-mail address: liquan@phy.cuhk.edu.hk (Q. Li).

https://doi.org/10.1016/j.jpowsour.2017.11.084
Received 10 August 2017; Received in revised form 2 November 2017; Accepted 26 November 2017

capacity decay of SnS. Replacing the commonly employed acetylene black (AB) conductive additive by multi-wall carbon nanotubes (MWCNT) during electrode preparation led to largely improved capacity retention at 50th cycles (from 67% in the case of AB to 84% in the case of MWCNT). Such improvement correlates well with the observed suppression of both Sn agglomeration and Na_2S enrichment during cycling. We also demonstrated that P2-$Na_{2/3}Ni_{1/3}Mn_{1/2}Ti_{1/6}O_2$/SnS-MWCNT full cell delivers a first capacity of 100 mAh/g (based on total mass of cathode and anode) with an average discharge voltage of 3.62 V, corresponding to an energy density of 262 Wh/kg. The full cell retains 71% of its initial capacity after 40 cycles.

2. Experimental

2.1. Preparation of the SnS and P2-$Na_{2/3}Ni_{1/3}Mn_{1/2}Ti_{1/6}O_2$

All reagents are analytical grade and used without further purification.

In a typical procedure for the preparation of SnS nanosheets, 0.9 g thiourea, 1.36 g $SnCl_2{\cdot}2H_2O$ and 60 mL anhydrous ethylene glycol (EG) were added to a beaker in air. The mixture was treated with mild magnetic stirring for 5 min before being transferred into a 100 mL stainless steel Teflon-lined autoclave. The autoclave was sealed and the temperature was maintained at 160 °C for 8 h before being cooled down to room temperature. The precipitate was separated by centrifugation, washed with distilled water and absolute ethanol several times, and finally vacuum dried at 60 °C for 4 h.

P2-$Na_{2/3}Ni_{1/3}Mn_{1/2}Ti_{1/6}O_2$ was prepared by solid state reaction using Na_2CO_3, NiO, Mn_2O_3, and TiO_2 as raw materials. A stoichiometric mixture amount of raw material was mixed by ball mill at 200 rpm for 6 h. And the mixture was dried, heated at 900 °C for 20 h followed by quench in air.

2.2. Characterizations

The crystallinity of the samples was examined by X-ray diffraction (XRD, SmartLab, Rigaku) with a Cu Kα radiation source (λ = 0.1541 nm). The XRD patterns of SnS and the electrodes were collected with a scan rate of 8°/min under 40 kV and 40 mA, and a scan rate of 0.2°/min under 40 kV and 80 mA, respectively. To avoid any possible exposure to air, the electrodes were sealed by 2 mil Kapton tape in argon-filled glove box before transporting to XRD experiments. And all electrodes subjected to ex-situ XRD have similar loadings. The morphologies of the samples were characterized by a field emission scanning electron microscope (FESEM, Quanta 200, FEI). Transmission electron microscopy (TEM FEI Tecnai F20ST) equipped with an energy dispersive spectrum X-ray detector (EDS) were carried out to study the detailed microstructure and spatial distribution of the compositional elements in the respective samples. X-ray photoelectron spectroscopy (XPS) was collected with Al Kα radiation on a PHI Model 5802 (calibrated with C 1s at 284.8eV [9]) to evaluate the oxidation states of Sn and S in the as-synthesized SnS. The fine scan of each element was collected with steps of 0.1eV and pass energy of 55eV. N_2 adsorption and desorption isotherm (ADI) were collected by the ASAP 2000 after the sample was vacuum dried at 120 °C for 6h [10].

2.3. Electrodes preparation

The anode electrodes were prepared by mixing SnS (active material) with conductive additives (either AB or MWCNT; and the corresponding electrodes are named as SnS-AB electrode or SnS-MWCNT electrode depending on the conductive additives employed) and sodium carboxymethyl cellulose (NaCMC) binder with a mass ratio of 80:10:10 in water to form homogeneous slurry. The slurry was then coated on Cu foil followed by a vacuum drying at 60 °C overnight. Electrodes with diameter of 16 mm and active material loading of ~1.5 mg/cm^2 were then cut out from the dried coating.

The cathode electrodes casted on Al current collector were prepared using 80 wt% P2-$Na_{2/3}Ni_{1/3}Mn_{1/2}Ti_{1/6}O_2$ active material, 10 wt% AB and 10 wt% poly(vinylidene fluoride) in n-methyl-2-pyrrolidone solvent. The electrodes are vacuum dried at 90 °C and then cut out with diameter of 16 mm.

2.4. Assembly of cells and electrochemical measurements

The electrodes were assembled into CR2025 coin-type cells with Na foil and glass fiber filter (GD-120) as reference electrode and separator, respectively. 1 M $NaClO_4$ in a mixture of propylene carbonate and fluoroethylene carbonate (PC/FEC, 95:5, by volume) was used as the electrolyte.

For the full cell, the mass ratio of cathode and anode is about 3.79:1. And both electrode were activated for one cycle in a half-cell before being assembled into full cell.

The Na-ion cells were galvanostatically charged/discharged using multichannel battery test system (Neware, Shenzhen). 10 min of rest was employed between each charge and discharge process. Electrochemical impedance spectroscopy (EIS) was carried out via electrochemical workstation (CHI 760E, Shanghai Chenhua Instrument Co., Ltd.). All experiments were carried out at room temperature (24 ± 2 °C) unless specified otherwise.

3. Results and discussions

3.1. Material characterizations of the as-prepared SnS

Fig. 1a shows the XRD data of the as-prepared SnS. All diffraction peaks can be indexed to the orthorhombic SnS with space group of Pnma(62) (JCPDS#73–1859). SEM image shows that the as-prepared SnS are micron-sized three-dimensional flower-like structures assembled by nano-sheets.

Fig. 1c shows a typical low magnification TEM image of the sample, revealing an individual nano-sheet. A selected area electron diffraction pattern taken from such a nano-sheet is shown in Fig. 1d, which can be index to [010] zone axis of orthorhombic SnS. The spatial distribution of the compositional elements is revealed by EDX maps taken from part of the flower-like sample (Fig. 1e), showing the uniform distributions of Sn and S in as-prepared SnS. XPS (Fig. S1) confirms the valance state of Sn and S in the as-synthesized SnS as +2 and −2, respectively. The results are consistent with the literature report of SnS [11,12].

To investigate the pore structure of the flower-like materials, N_2 ADI of the as-prepared SnS was collected (Fig. 2). The N_2 ADI displays a typical type-III curve with H3 hysteresis loop, indicating the presence of slit-like mesopores in aggregates consisting of plate-like particles [13,14], which is consistent with SEM image. BET (Brunauer-Emmett-Teller) surface area was determined to be 41.0 m^2/g by the N_2 ADI.

3.2. Capacity fading mechanism of SnS

The capacities of the SnS electrode with AB as the electronic conductive additive measured at a current density of 100 mA/g are plotted as a function of the cycle numbers, as shown in Fig. 3a. The first sodiation/de-sodiation capacities are 579.2 and 424.3 mAh/g, respectively, corresponding to an initial coulombic efficiency (ICE) of 73.3%. The first irreversible capacity loss could be explained by the formation of solid-electrolyte interface (SEI) layer [15,16], and the SEI is expected to suppress the continuously electrolyte decomposition upon subsequent cycles, which is supported by the significantly increased coulombic efficiency in the next several cycles (Fig. S5). After 50 cycles, the electrode only delivers ~67% of first de-sodiation capacity (*i.e.* 284.3 mAh/g).

The change in electrochemistry along with capacity decay is suggested by the evolution of de-sodiation voltage profile upon cycling.

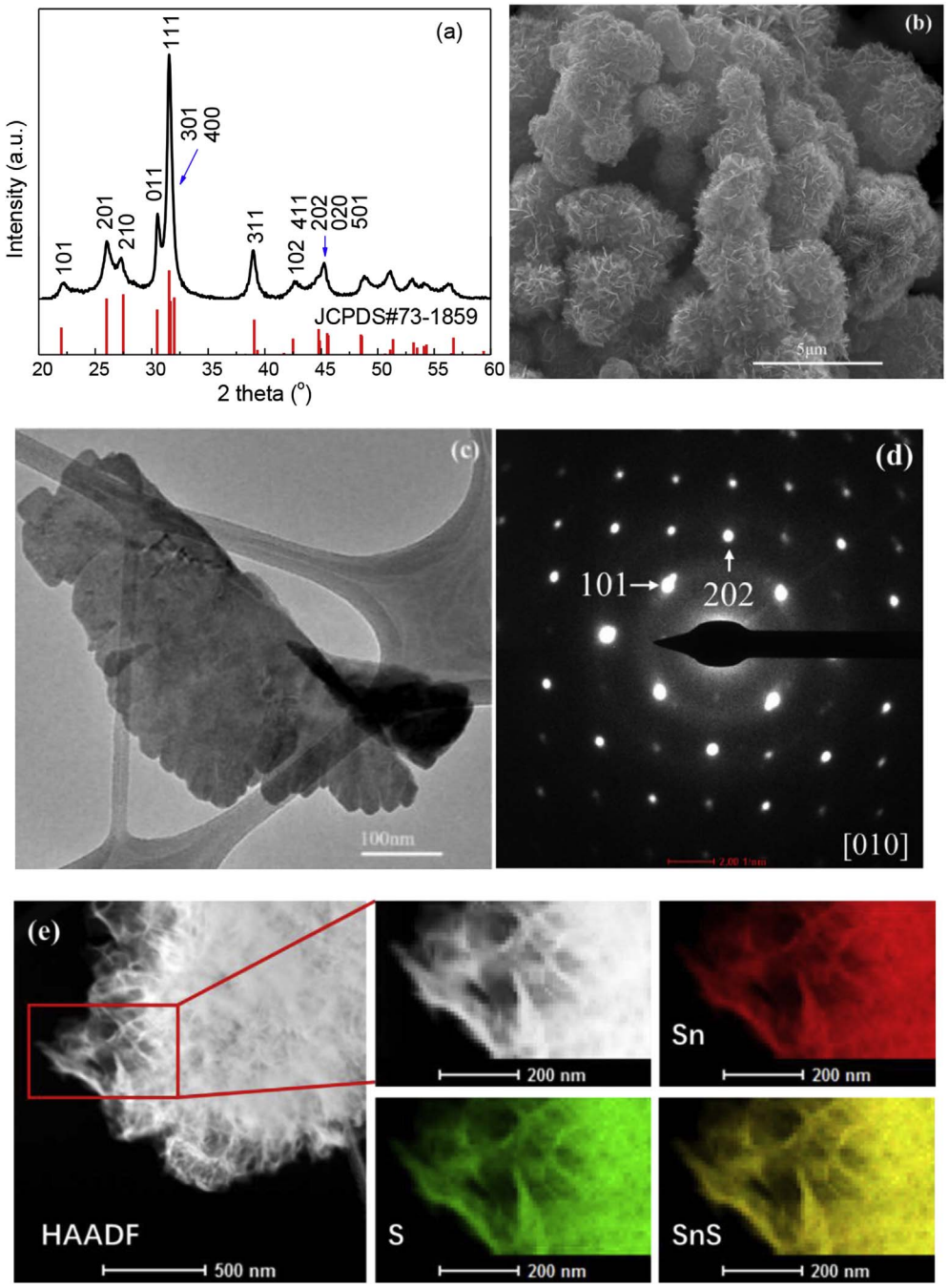

Fig. 1. (a) XRD pattern of the as-prepared SnS, (b) SEM image of the as-prepared SnS, (c) low magnification TEM image of SnS nano-sheet, (d) selected area electron diffraction pattern from a single layer SnS nano-sheet, (e) high-angle annular dark-field (HAADF) image and the corresponding scanning energy dispersive X-ray spectroscope (EDX) elemental maps of Sn, S and their overlapped image.

The 2nd de-sodiation voltage profile shows a sloping voltage plateau at ~0.25 V. After 20 cycles, the voltage plateau at ~0.25 V becomes obvious, and a second one appears at ~0.8 V, together with an obvious capacity loss above 1.2 V. With extended cycles, the two voltage plateaus become more prominent and significant capacity loss occurs above 1.2 V. The redox reaction of SnS anode for SIB has been well-documented in the literature [4], *i.e.*, (i) $SnS + 2Na^+ + 2e^- \leftrightarrow Sn + Na_2S$; and (ii) $Sn + xNa^+ + xe^- \leftrightarrow Na_xSn$. The thermodynamic equilibrium voltage (or termed electromotive force, emf) for reaction (i) is ~1.30 V *vs.* Na/Na^+ based on the Gibbs energies of SnS formation (−98.3 kJ/mol) and Na_2S (−349.8 kJ/mol) [17]. While the emf for reaction (ii) should be lower than 0.8 V *vs.* Na/Na^+ based on the results of Sn anode for SIB [18,19]. Therefore, the capacity loss above 1.2 V should mainly originate from the continuously deteriorated reconversion from Sn and Na_2S to SnS. In addition, the de-sodiation voltage profiles of SnS after 20 cycles resembles that of pure Sn electrode (Fig. S7) while the little variation of Sn/S atomic ratio is observed after charge/discharge cycles (Fig. S8). These results suggest the presence of physical mixing of Sn and S (and/or Na_2S), instead of SnS, in the de-sodiated electrode after repeated cycles.

XRD (Fig. 3c) of the electrodes taken after different number of cycles (at 2.0 V) were collected to investigate the phase/structure change of the SnS electrode upon cycling. After the first cycle, all diffraction peaks of SnS (including the highest one at ~31.5°) disappear completely and little signal of Sn can be detected, suggesting the final de-sodiated materials after the first cycle are composed of small grains in highly dispersed states [20,21]. After 20 cycles, a new set of diffraction peaks of tetragonal Sn (JCPDS#04–0673) appears, indicating the segregation of crystalline Sn from SnS. After 50 cycles, increased diffraction intensity from Sn and the narrowed diffraction peak width indicate

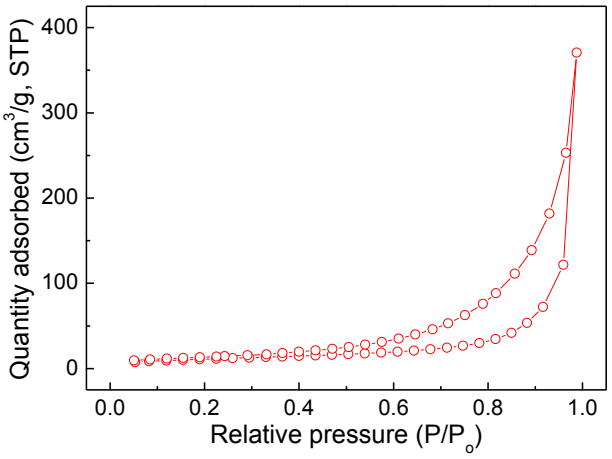

Fig. 2. N_2 adsorption and desorption isotherm of the as-prepared SnS.

the continuously agglomeration of Sn (grain growth) in the electrode. At the same time, the appearance of dominant diffraction signal at ~38.9° after 50 cycles can be ascribed to Na_2S, indicating that some Na_2S are formed during sodiation, and is partially irreversible in the following de-sodiation process. This enrichment of Na_2S at the end of the de-sodiation process suggests the increased difficulty in Na_2S de-sodiation and the SnS reconversion upon cycling. These results are consistent with the analysis of electrochemical results shown in Fig. 3a and b.

3.3. Improving cycle stability by limiting Sn agglomeration

Seeking an effective approach to suppress Sn agglomeration and enrichment of Na_2S upon repeated cycles, we attempted to employ MWCNT instead of AB as the conducting additive to the electrode. This is inspired by the literature report of CNT employed in LIB. The presence of CNT has been suggested to suppress Sn aggregation, and was indeed found to improve the cycle performance of Sn anode in LIB [22–24].

Simply by replacing AB with MWCNT as electronic conductive additive during electrode preparation, the capacity retention of SnS electrode over 50 cycles is largely increased from 67% to 84% (Fig. 4a).

To understand the improved cycle stability, we study the evolution of voltage profiles and ex-situ XRD patterns of SnS-MWCNT electrode. As can be seen from Fig. 4b, little change can be detected in the characteristics of the voltage profiles of SnS-MWCNT electrode upon cycling, although some capacity decay occurs after 20 cycles. The similar characteristic in the de-sodiation voltage profile of the electrodes upon cycling suggest similar composition of the electrode material in these cycles, that is to say, reformation of SnS likely occurs after each de-sodiation process. Moreover, the voltage profiles are generally lack of plateaus features even after 50 cycles, suggesting the small gain size of the active material and reduced agglomeration of Sn. This is also supported by ex-situ XRD data of the electrodes after different cycles (Fig. 4c). Only broad diffraction peaks of Sn with low intensity are detected even after 50 cycles. At the same time, the diffraction intensity of Na_2S remains low, indicating its small population. These results suggest that MWCNT effectively suppress Sn agglomeration and likely promote the formation of SnS upon repeated cycling, and thus improves the cycle stability of the SnS electrode, which is also consistent with the

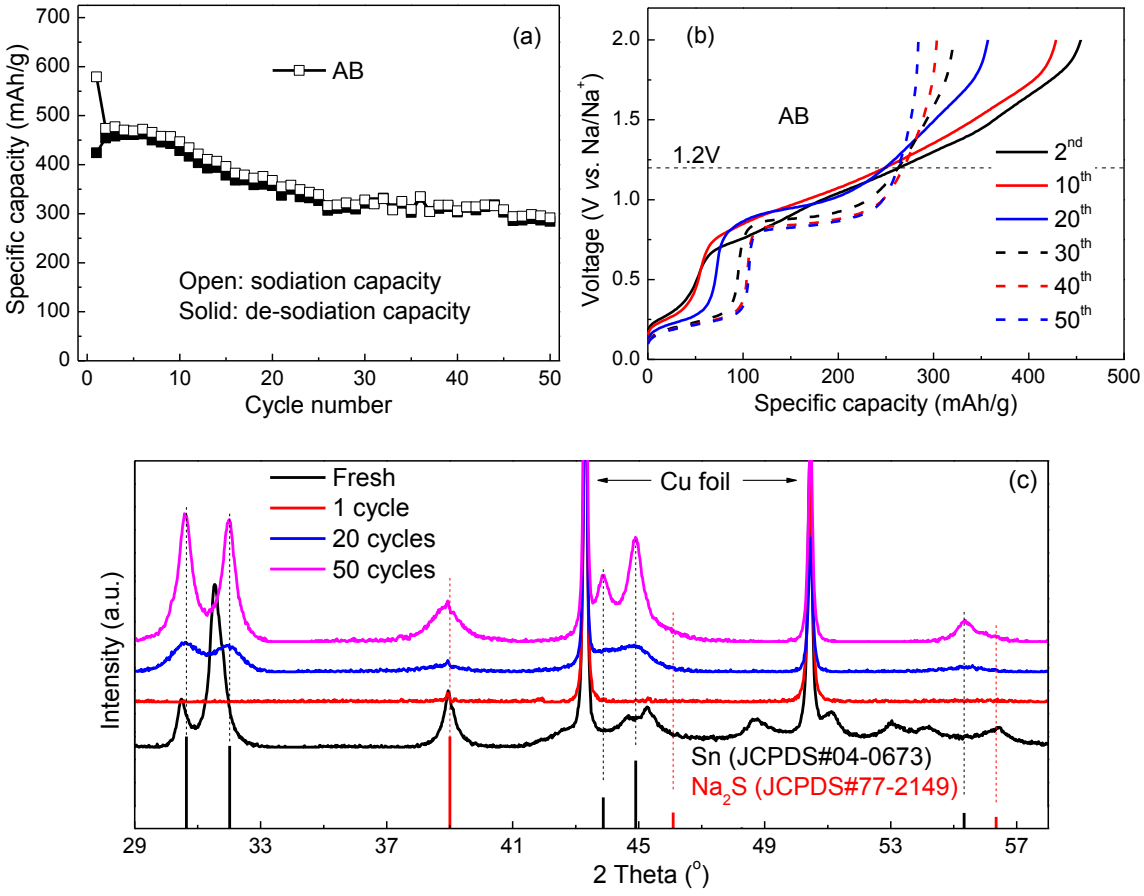

Fig. 3. (a) Cycle performance and (b) evolution of de-sodiation voltage profiles of SnS-AB electrode cycled in 2.0–0.01 V at 100 mA/g; (c) the ex-situ XRD patterns of the SnS-AB electrode after cycling for specific cycles.

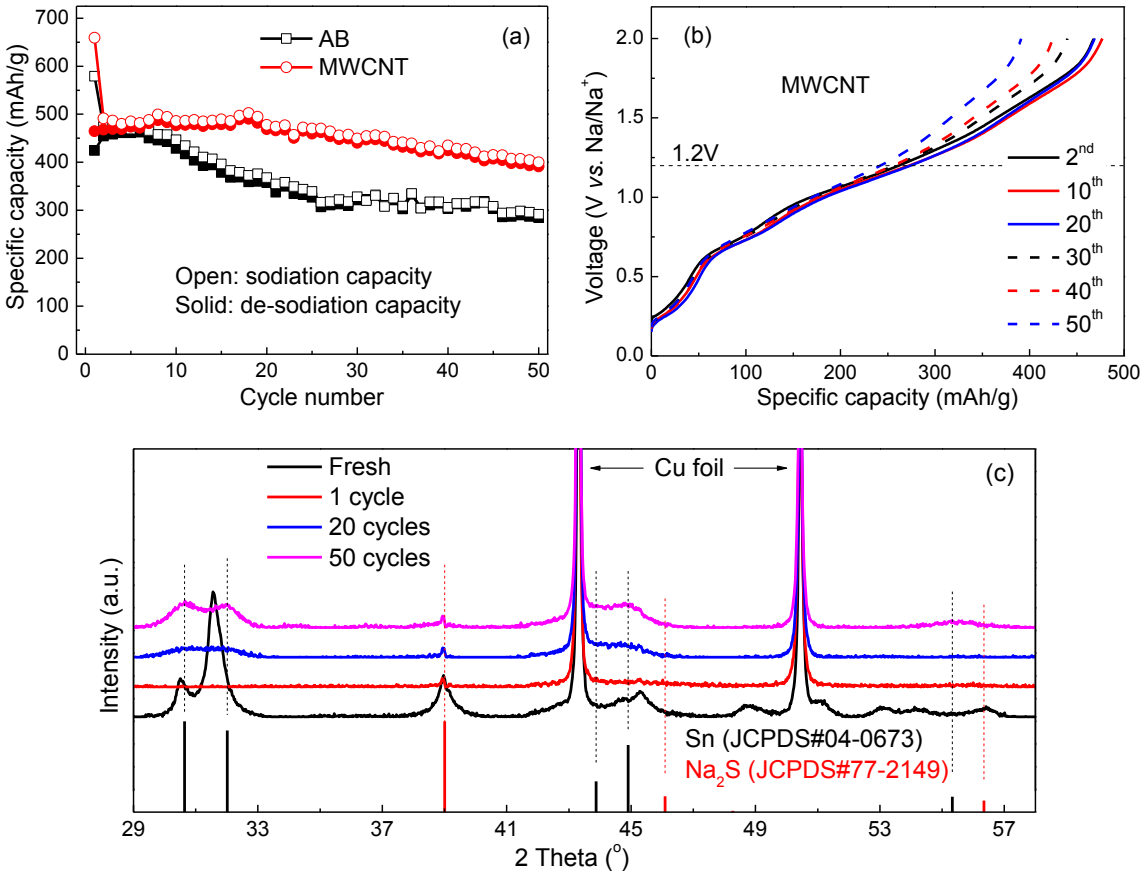

Fig. 4. (a) Comparison of cycle performance of SnS-AB electrode and SnS-MWCNT electrode cycled in 2.0–0.01 V at 100 mA/g; (b) evolution of de-sodiation voltage profiles of SnS-MWCNT electrode cycled in 2.0–0.01 V at 100 mA/g; (c) the ex-situ XRD patterns of the SnS-MWCNT electrode after different charge/discharge cycles.

EIS evolution of electrodes shown in Fig. S9.

Fig. 5 presents the rate capability of the SnS-MWCNT electrode. The SnS-MWCNT electrode can deliver de-sodiation capacities of 450.0, 441.9, and 410.3mAh/g when being charged/discharged at current density of 100, 200, and 500 mA/g, respectively; and 459.9mAh/g can be recovered immediately after resetting the current density to 100 mA/g. The high rate capability can be attributed to the effective and robust conducting network provided by MWCNT and little Sn agglomeration from pristine SnS-MWCNT electrode.

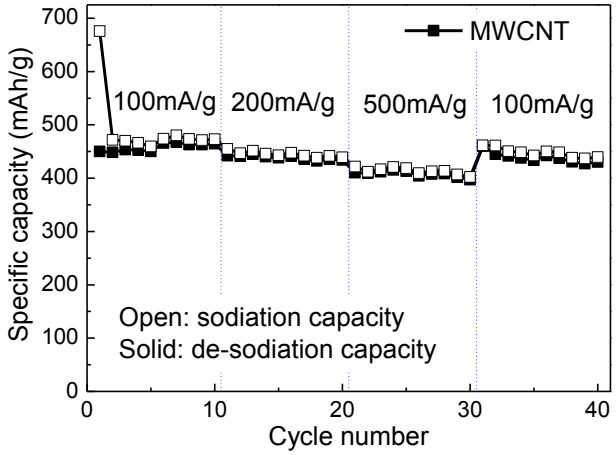

Fig. 5. Rate capability of SnS-MWCNT electrode cycled in 2.0–0.01 V.

3.4. Electrochemical performance of SnS electrode in full cell

We further evaluated electrochemical performance of SnS electrode in a sodium-ion full battery with P2-$Na_{2/3}Ni_{1/3}Mn_{1/2}Ti_{1/6}O_2$ as the positive electrode [2,25]. The electrochemical performance of P2-$Na_{2/3}Ni_{1/3}Mn_{1/2}Ti_{1/6}O_2$ electrode is shown in Fig. S10. The full cell was charged/discharged in a voltage range of 0.9–4.3 V at 0.1C (~13mA/g-cathode), and the results are shown in Fig. 6. The full cell with SnS-MWCNT anode delivers a first discharge capacity of 100mAh/g (capacity normalized to total weight of cathode and anode) with an average discharge voltage of 2.62 V, which corresponds to an energy density of 262 Wh/kg. Furthermore, the P2-$Na_{2/3}Ni_{1/3}Mn_{1/2}Ti_{1/6}O_2$/SnS-MWCNT full cell demonstrates a good capacity retention of 71% over 40 cycles, which is significantly higher that of P2-$Na_{2/3}Ni_{1/3}Mn_{1/2}Ti_{1/6}O_2$/SnS-AB full cell (45%).

4. Conclusion

Progressive agglomeration of Sn and enrichment of Na_2S at the end of de-sodiation process are observed during the capacity fading of the SnS electrode. Employing MWCNT, instead of AB as the conductive additive, is found to largely improve the cyclability of the SnS electrode by suppressing the Sn agglomeration and likely promoting the re-formation of SnS. SnS-MWCNT electrode can deliver a capacity of 465mAh/g with a capacity retention of 84% over 50 cycles. When pairing SnS-MWCNT electrode with P2-$Na_{2/3}Ni_{1/3}Mn_{1/2}Ti_{1/6}O_2$ cathode, the full cell can obtain an initial energy density of 262 Wh/kg with capacity retention of 71% after 40 cycles.

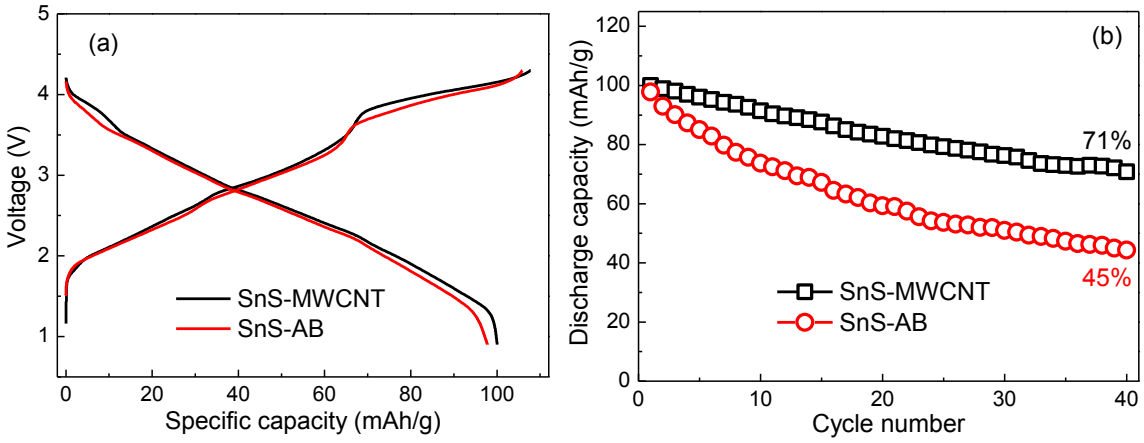

Fig. 6. The electrochemical performance of P2-$Na_{2/3}Ni_{1/3}Mn_{1/2}Ti_{1/6}O_2$/SnS full cell cycled in voltage range of 0.9–4.3 V at 0.1C (~ 13mA/g-cathode). (a) First charge/discharge curves, and (b) cycle performance. The capacity is normalized to the total mass of both cathode and anode materials.

Acknowledgments

This work is supported by RGC/GRF under project No. 14316716.

Appendix A. Supplementary data

Supplementary data related to this article can be found at http://dx.doi.org/10.1016/j.jpowsour.2017.11.084.

References

[1] H. Pan, Y.-S. Hu, L. Chen, Energy & Environ. Sci. 6 (2013) 2338.
[2] N. Yabuuchi, K. Kubota, M. Dahbi, S. Komaba, Chem. Rev. 114 (2014) 11636–11682.
[3] P.K. Dutta, U.K. Sen, S. Mitra, RSC Adv. 4 (2014) 43155–43159.
[4] T. Zhou, W.K. Pang, C. Zhang, J. Yang, Z. Chen, H.K. Liu, Z. Guo, ACS nano 8 (2014) 8323–8333.
[5] L. Ji, P. Meduri, V. Agubra, X. Xiao, M. Alcoutlabi, Adv. Energy Mater. 6 (2016) 1502159.
[6] L. Wu, X. Hu, J. Qian, F. Pei, F. Wu, R. Mao, X. Ai, H. Yang, Y. Cao, J. Mater. Chem. A 1 (2013) 7181.
[7] Y.C. Lu, C. Ma, J. Alvarado, N. Dimov, Y.S. Meng, S. Okada, J. Mater. Chem. A 3 (2015) 16971–16977.
[8] E. Cho, K. Song, M.H. Park, K.W. Nam, Y.M. Kang, Small 12 (2016) 2510–2517.
[9] N. Zhang, C. Chen, X. Yan, Y. Huang, J. Li, J. Ma, D.H.L. Ng, Electrochimica Acta 223 (2017) 39–46.
[10] W. Wang, J. Zhang, Y. Lin, F. Ding, Z. Chen, C. Dai, Electrochimica Acta 170 (2015) 269–275.
[11] Y. Zheng, T. Zhou, C. Zhang, J. Mao, H. Liu, Z. Guo, Angew. Chem. Int. Ed. Engl. 55 (2016) 3408–3413.
[12] J. Wang, Y. Lu, N. Zhang, X. Xiang, J. Liang, J. Chen, RSC Adv. 6 (2016) 95805–95811.
[13] K.S. Sing, Pure Appl. Chem. 57 (1985) 603–619.
[14] Q. Xiang, J. Yu, W. Wang, M. Jaroniec, Chem. Commun. (Camb) 47 (2011) 6906–6908.
[15] L. Ji, Z. Lin, M. Alcoutlabi, X. Zhang, Energy & Environ. Sci. 4 (2011) 2682.
[16] V.A. Agubra, L. Zuniga, D.D. la Garza, L. Gallegos, M. Pokhrel, M. Alcoutlabi, Solid State Ionics 286 (2016) 72–82.
[17] J.A. Dean, N.A. Lange, Lange's Handbook of Chemistry, fifteenth ed., Mc-Graw-Hill Inc., New York, 1999.
[18] L.D. Ellis, T.D. Hatchard, M.N. Obrovac, J. Electrochem. Soc. 159 (2012) A1801–A1805.
[19] S. Komaba, Y. Matsuura, T. Ishikawa, N. Yabuuchi, W. Murata, S. Kuze, Electrochem. Commun. 21 (2012) 65–68.
[20] Y.-U. Kim, C.K. Lee, H.-J. Sohn, T. Kang, J. Electrochem. Soc. 151 (2004) A933.
[21] B. León, J.I. Corredor, J.L. Tirado, C. Pérez-Vicente, J. Electrochem. Soc. 153 (2006) A1829.
[22] M.-S. Park, S.A. Needham, G.-X. Wang, Y.-M. Kang, J.-S. Park, S.-X. Dou, H.-K. Liu, Chem. Mater. 19 (2007) 2406–2410.
[23] J. Zheng, S. Nai, M.-F. Ng, P. Wu, J. Wei, M. Gupta, J. Phys. Chem. C 113 (2009) 14015–14019.
[24] C.-j. Liu, H. Huang, G.-z. Cao, F.-h. Xue, R.A. Paredes Camacho, X.-l. Dong, Electrochimica Acta 144 (2014) 376–382.
[25] H. Yoshida, N. Yabuuchi, K. Kubota, I. Ikeuchi, A. Garsuch, M. Schulz-Dobrick, S. Komaba, Chem. Commun. 50 (2014) 3677–3680.